Ripening processes in supported and pinned nanoclusters—experiment, simulation and theory

2003 J. Phys.: Condens. Matter 15 S3139

(http://iopscience.iop.org/0953-8984/15/42/011)

INSTITUTE OF PHYSICS PUBLISHING JOURNAL OF PHYSICS: CONDENSED MATTER

J. Phys.: Condens. Matter **15** (2003) S3139–S3152 PII: S0953-8984(03)64560-1

Ripening processes in supported and pinned nanoclusters—experiment, simulation and theory

R A Bennett, D M Tarr and P A Mulheran

Department of Physics, University of Reading, Reading RG6 6AF, UK

Received 6 June 2003, accepted for publication 11 July 2003
Published 10 October 2003
Online at stacks.iop.org/JPhysCM/15/S3139

Abstract

We have investigated experimentally and theoretically the role that ripening processes play in the evolution of supported transition metal nanoclusters on solid surfaces. We discuss some avenues of analysis that can be more informative of the dominant mechanisms than mere temporal measures of island size. Our model system is formed by the growth of Pd nanoclusters at room temperature on the cross-linked (1×2) reconstructed $TiO_2(110)$ surface. The reconstructed surface contains a rectangular array of 'defects' that nucleate and pin the clusters. We have followed the surface evolution by variable temperature scanning tunnelling microscopy as the temperature was raised stepwise to 973 K. We find that the ripening is dominated by an Ostwald-type mechanism with particles remaining immobile during growth (decay). Monte Carlo simulations of the ripening of arrays of three-dimensional islands have been undertaken for comparison with the experiments. These reproduce the spatial properties of the experimental arrays and the scaling nature of the height distribution. In addition the classic mean field theory for the size distribution is modified to include island size-separation correlations and is found to recover the size distribution found in both the simulation and the experiment. We conclude that detailed atomistic understanding of ripening is not always necessary to understand important features of nanostructure evolution.

M This article features online multimedia enhancements

1. Introduction

Ripening processes are ubiquitous in many areas of scientific research, from understanding solid state crystal growth to the aggregation of proteins [1]. In particular the ripening of supported metal catalysts has been extensively studied [2] with many mechanisms postulated to explain the time dependent behaviour of the mean particle size and density. Two classes of mechanism are of direct relevance here: coalescence sintering and Ostwald ripening [3]. In the

former case this involves the merging of two clusters that momentarily touch (either through growth or diffusion of one or other cluster) to form a single larger entity; in the latter continuous evaporation onto the substrate from the clusters and re-condensation of these adatoms onto the clusters occur, leading to a threshold cluster size above which clusters grow and below which clusters shrink. These mechanisms have traditionally been identified through the cluster number density derived from conservation of mass, and through comparison with theoretical predictions for the power law dependence of the mean island size:

$$\langle r(t)\rangle^n - \langle r(0)\rangle^n = Kt. \tag{1}$$

Here $\langle r(t)\rangle$ is the mean island radii at time $= t$, K is a temperature and material dependent constant and n is an integer determined by the prevalent mechanism.

For Ostwald ripening mean field theory predicts $n = 3$ or 4 depending on whether the rate limiting step is detachment of the atom from a cluster or diffusion of the adatom on the surface. For diffusion coalescence the mechanisms that underlie the diffusion event dominate the dependency, with $n = 7$ predicted for diffusion and coalescence of spherical clusters. However, facetted clusters may diffuse much slower as a 'pillbox' of atoms reaching a critical size must first nucleate and grow on the leading facet, resulting in a non-simple growth law with exponents $n > 7$ which may also change with time. Exponents n between 15 and 2 have been found in experimental studies of sintering in real catalysts in various atmospheres (see examples given in [2]) and the relative strengths of coalescence and Ostwald regimes have been investigated theoretically [4].

Recent advancements have been made through measurement of arrays of particles grown and supported on well-defined single crystal metal oxide surfaces by scanning tunnelling microscopy (STM). These model catalysts benefit from simplified interactions due to the vacuum environment, uniform substrates and uniform loading. The diffusion coalescence mechanism was identified in the case of Pd on $TiO_2(110)$ for very small (mean size < 50 atoms) Pd particles [5]. These authors noted, however, that in this regime it is not possible to distinguish Ostwald ripening from diffusion coalescence solely on the basis of the measured growth law, relying upon detailed particle size distributions and *in situ* observation of cluster diffusion (at room temperature) to draw conclusions. Ostwald ripening was suggested to be active after observation, by direct STM imaging at temperature, of the evolution of a strongly bimodal size distribution of Pd on (1×1) oriented TiO_2. Direct observation at temperature has also been employed to image Au nanoclusters on $TiO_2(110)$ at 750 K [6]. In this case the authors observe rare diffusion and coalescence events in 50 Å diameter clusters, some nucleation events on bare terraces and some unquantified growth of large clusters. They conclude diffusion coalescence is present yet classical Ostwald ripening is dominant, as evidenced by static growth of clusters and the presence of adatoms on terraces.

These previous studies show that analyses other than the growth exponents of equation (1) are necessary to elucidate dominant mechanisms of evolution, a conclusion reinforced in this present work. Here we shall look at the statistical properties of the spatial ordering in ripening nanostructure arrays, as well as height distributions, which has consequences for applications in technology. We present data for *in situ* observation at 873 K of larger Pd nanoparticles supported on a cross-linked (1×2) reconstructed $TiO_2(110)$ surface. This novel surface contains well-defined periodic sites at the cross-links of the reconstruction [7] that provide nucleation sites for the clusters during growth. Such nucleation sites are often implicated in growth studies on oxides [8] but are rarely so well characterized, one notable exception being the role of oxygen vacancies [9]. Very recently there have been several reports suggesting that clusters above a critical size are capable of de-pinning from the defect to become mobile on the surface [10], although clear experimental evidence for this is lacking due to the range of

uncharacterized defects present, leading to a wide distribution of de-pinning sizes. We do not observe any mobile clusters on this surface at 873 K.

Motivated by the experimental results we have also conducted a simulation study of nanostructure ripening. Due to the complexity of the growth exponent analysis, which does not give clear guidance to the atomistic details of the ripening mechanism, we focus on the spatial aspects of the ripening arrays and employ a simple 'coarse-grained' Monte Carlo simulation. We find that the simulations show asymptotic scaling consistent with the experimental data, and we also present a new theory for the island size distribution observed in the simulation and experiment. The study leads us to a dramatic conclusion: even starting with an ordered array of nanostructures the system evolves into the same 'partially disordered' state as any disordered starting array would. This is the power of the scaling properties of ripening processes, which appear to have only one final 'attractor' for the spatial ordering.

2. Experimental details

The experiments were performed on a W A Technology variable temperature STM (VT-STM) that has been described in detail before [11]. The $TiO_2(110)$ single crystal (PiKem, UK) was cleaned by standard Ar^+ ion sputter and anneal methods to produce an atomically clean cross-linked (1×2) reconstructed surface. Pd was deposited on the surface at room temperature from an uncalibrated thermal evaporation source that was thoroughly outgassed prior to use. The surface coverage of Pd atoms is thought to be of the order of 1 ML with respect to the number of Ti ions in the surface. The temperature was raised in systematic increments with images taken once the temperature had stabilized.

Images presented here were taken at temperature, often rapidly after a significant temperature jump (for example within 226 s after a temperature jump from 773 to 873 K). For the jump experiments the initial few images were subject to some random lateral thermal drift which distorted the particle morphology and introduced some noise into the measurement of particle density. Within 1000 s this had settled sufficiently to allow images to be taken at small scan size with negligible distortion, manual corrections to imaging position were made of the order of 20 Å between images to maintain true surface position. Hence we present particle density data for the full range that was measured and particle dimensional data where valid.

When imaging three-dimensional structures by scanning probe microscopy the finite size of the tip can potentially distort lateral dimensions. This effect was noticeable on re-establishing tunnelling after the tip had been withdrawn for a considerable period of time; images taken immediately tended to have extended particle dimensions while height data was unaffected. As a result we present the height and density of the particles as our primary source of data as these parameters are unaffected by tip shape. We also present secondary data on the lateral dimensions of the particles that may be affected by tip shape but where no influence is perceptible. The discussion of lateral dimensions will therefore be limited to time dependencies and comparison of the long and short axes of the particles in which tip shape results in little distortion of the particle morphology. Particle sizes are measured using semi-automated identification and data reduction software written in-house. Particle heights are measured from the maximum height of the particle to the mean height of the terrace at the periphery of the cluster. Thus particles resting at step edges have heights intermediate to measurements with respect to either terrace.

3. Evolution mechanisms and growth exponents

Figure 1 shows characteristic VT-STM images of Pd nanoparticles grown at 300 K on the cross-linked (1×2) surface and imaged *in situ* as the array ripens at the temperatures indicated

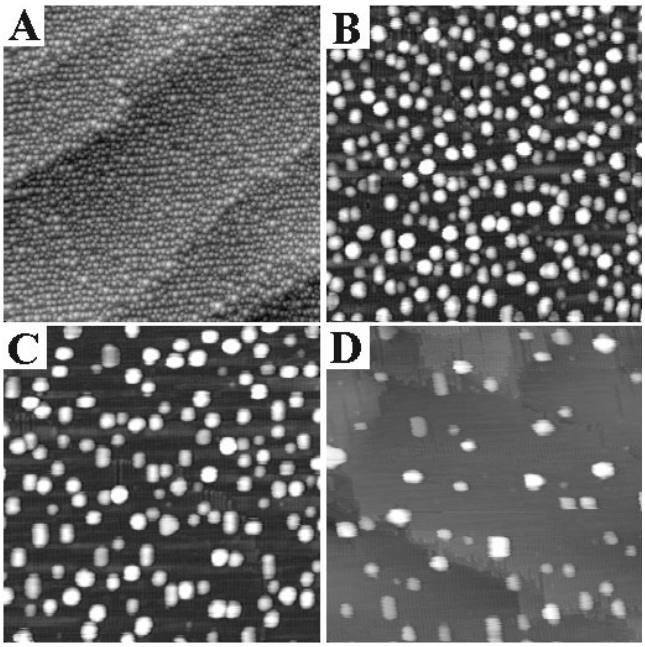

Figure 1. Variable temperature STM images of a Pd loaded cross-linked (1 × 2) reconstructed TiO_2(110) surface. (A) 1500 Å square image taken at 373 K showing the regular arrangement of nanoparticles that have nucleated on the cross-link sites. The step edges do not significantly perturb the array. (B) 1000 Å square image at 773 K showing significant ripening with little residual spatial order. (C) 1000 Å square image at 873 K showing the evolution of a range of differing nanoparticles geometries. (D) 1000 Å square at 973 K showing the range of particle morphologies and the underlying step structure of the reconstructed surface.

in the caption. At low temperature (A) there is a significant ordering of the array that is dictated by the lattice of nucleation sites on the substrate [12]. The step edges, running diagonally, only weakly perturb the spatial ordering. As the temperature is increased (B)–(C) in a stepwise manner and held the array ripens and becomes less ordered. There is no perceptible change in the substrate structure up to 973 K (D) where the cross-linked (1 × 2) is clearly visible. Images (A) and (D) are unprocessed (apart from a linear background subtraction in the fast scan direction) so that the step structure of the underlying substrate is visible. Images (B) and (C) have been processed in a similar manner to that described in [13] such that the step structure is subtracted leaving a clearer impression of the range of heights in the image. All statistical results are derived from the unprocessed data.

Upon annealing the array evolves to a lower nanoparticle density (figure 2) at a rate which is sensitive to the surface temperature. For temperatures up to and including 873 K the rate increases with temperature; at 973 K however the characteristic exponent falls significantly. The changing exponent shows the complexity of the ripening with no single classical mechanism operating at all temperatures. Due to the very slow rates of ripening at low temperatures we shall concentrate here on the most extensive data at 873 K.

Figures 3(A)–(F), imaged at 873 K, shows the static coalescence of two nanoparticles of height 7.0 and 10.4 Å to form a single extended cluster of ∼7.5 Å height. In (A) the particles are clearly resolved as separate entities; 3 min later, (B), the particles outlines are beginning to merge although a clear dividing line is seen between clusters. In (C) and (D) the smaller particle

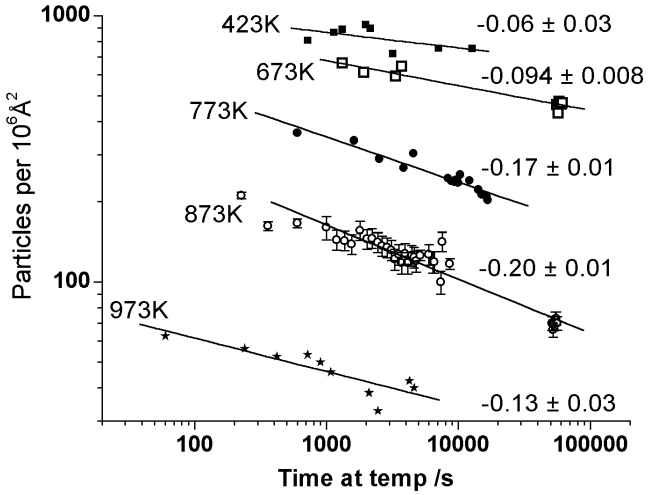

Figure 2. Particle density versus annealing time at various temperatures, all imaged *in situ* at temperature. The straight lines are linear least square fits to determine exponents as shown.

appears to be spreading to form a skirt around the larger which in turn is shrinking in lateral dimensions; after 12 min, (E), a roughly square shape has formed that evolves into an facetted irregular polygon, (F). The clusters do not appear to have coalesced through a diffusion event as the centre of mass appears fixed. It is probable that a shape fluctuation or growth through another ripening mechanism lead to closely neighbouring clusters momentarily touching and this triggered the static coalescence. This minority event was observed during a sequence of images taken as soon after the heating step as possible (from 226 s). The full sequence of images, a representative sample of which are shown as figure 4, shows that coalescence is rare and that the evolution of the film is predominantly driven by the growth (decay) of well-spaced static clusters. A sequence imaging the same area of the surface has been put together as a movie and is included as stacks.iop.org/JPhysCM/15/S3139/mmedia.

Figure 4 shows six 1000 Å square images of the same area taken from a sequence of 36 at 873 K where the clusters can be seen to evolve with time. Particles indicated with an ellipse can be seen to decay with time, eventually disappearing; the circle shows the coalescence event from figure 3. Some particles vanish suddenly while others show a tendency to decay in subsequent frames. The decay of static particles with time is a characteristic of Ostwald ripening as material is transported across the surface from particles of high chemical potential (small radius) to lower chemical potential (larger radius). However, the particles that are observed to decay do not appear initially to be particularly small, especially close to larger neighbours or situated on a disordered surface (all factors expected to induce decay).

Figure 5 shows the mean height of decaying clusters (which were observable for reasonable lengths of time) versus the time before they decay. A range of particle sizes are seen to decay with different rates, the variation in height with time is also not smooth and has a rippled structure. This most probably results from nanoparticle shape changes during decay (such ripples are unlikely to be due to systematic variations in image analysis as they are not reproduced on other clusters in each image). Growth of particles from the mass transport is difficult to distinguish as small changes in height give rise to large changes in volume for large particles.

Figure 6 shows the evolution of particle height and number density with time. The mean particle height grows slowly as $\sim t^{+1/10}$ while the particle density drops more rapidly as $\sim t^{-1/5}$.

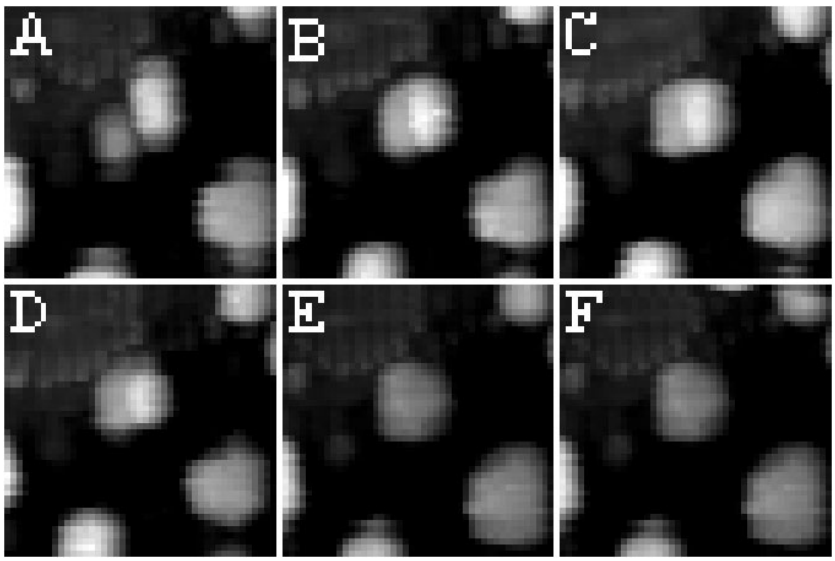

Figure 3. The static coalescence of two small Pd nanoparticles. (A)–(F) show the clusters at 3 min intervals. They initially start as clearly independent entities but rapidly come together to form a single larger particle.

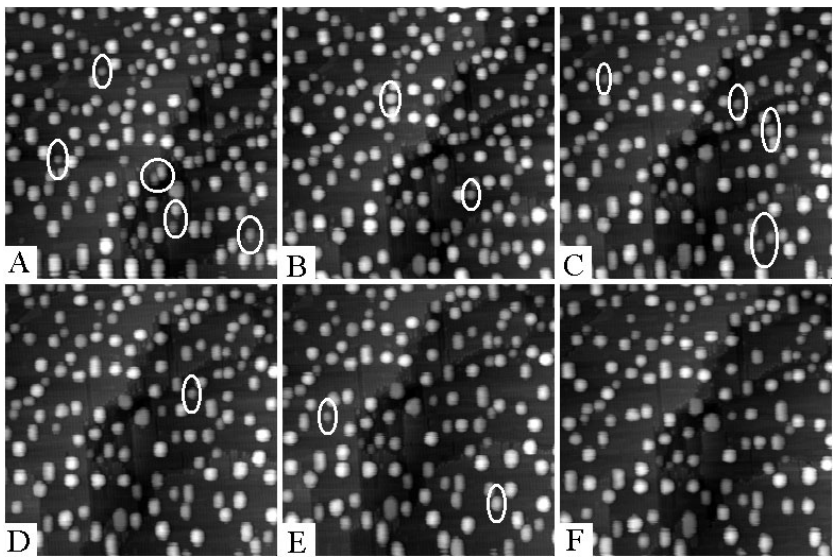

Figure 4. 1000×1000 Å images of the Pd nanoparticles ripening at 873 K taken sequentially after a temperature jump from 773 to 873 K. The circle highlights the coalescing pair of figure 3 while the ovals indicate particles that shrink and disappear in subsequent images.

Conservation of mass in this system (Pd is not lost to the TiO_2 bulk or gas phase) therefore dictates that the mean particle volume should increase as $t^{1/5}$. For particles that continuously change size, but not shape, the volume is proportional to the cube of any lateral dimension, in this case the height should change as $t^{1/15}$. This is clearly inconsistent with the data and so the assumption that particles change size but not shape continuously must be flawed. This

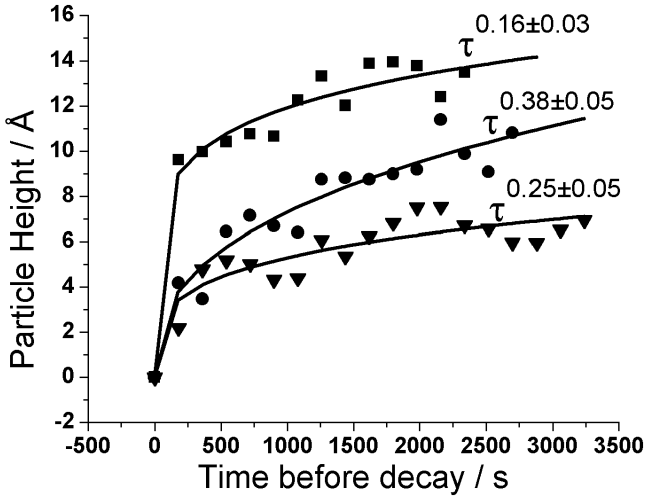

Figure 5. Shows the height of a selection of decaying clusters from the full sequence at 873 K as a function of time before disappearance. The curves represent best-fit simple power laws with a range of exponents. The periodic height changes in some of the data are probably due to shape changes of the particle.

is not unexpected as the particles strive to attain their equilibrium crystal shape every time an adatom attaches or leaves. This process of attaining a shape is omitted in the classical Ostwald ripening theory. The time taken to reshape has recently been included with regard to the growth of nanostructures, and in particular coalescence [14]. However, these models of coalescence are based upon a surface chemical potential argument [15, 16] which has limited validity. Kinetic Monte Carlo studies have shown that (free) clusters coalesce on much longer timescales with facets present as they can be trapped into metastable facetted structures while evolving to lower energy conformations [17]. The reshaping rate is limited by the time taken to nucleate a stable kernel on a pre-existing facet.

In support of a change in the average shape of the nanoparticles during ripening we have measured the lateral dimensions of the particles. We define the width as the maximum extent of the particle in the $\langle 1\bar{1}0\rangle$ direction and the length as the maximum extent in the $\langle 001\rangle$ direction of the substrate, both measurements being made from the areal centre of each particle. The length shows no strong dependence on time whereas the width grows in time until comparable to the length. This is a clear indication that the particles are reshaping in an attempt to attain their equilibrium crystal shape while undergoing ripening. This may be a rather slow process as clusters can become trapped in metastable conformations. Examples of this are given in figure 1(D) where the surface temperature has been raised to 973 K and the clusters imaged. Clearly there is a wide range of morphologies for clusters that have similar volumes indicating either a manifold of equilibrium crystal shapes or significant trapping into metastable structures. We believe the latter is more likely as the film is still undergoing ripening at this temperature.

The modification of the particle aspect ratio during ripening and its time dependence complete the description of the behaviour in this system. The number density falls as $t^{-1/5}$, the mean height grows as $t^{+1/10}$, mean width grows $\sim t^{+1/10}$ and mean length as t^0. Together these lead to conservation of mass on the surface in time and are dimensionally correct. These values are at variance with the predicted values of Ostwald ripening and are much closer to the slow rates expected for diffusion coalescence. The observations clearly show that the vast

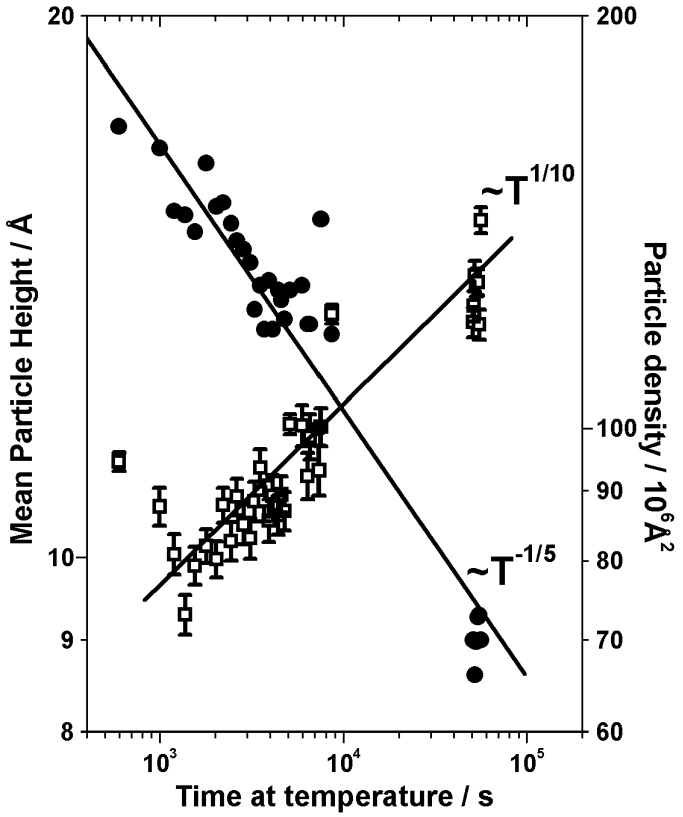

Figure 6. Shows the variation of particle density (dots) and mean height (open squares) as a function of annealing time at 873 K. The error bars are taken from the standard deviation of the height distribution.

majority of contributing particles are static implying the power law is not a good indicator of mechanism. Hence, we turn our attention to the individual properties of the clusters, rather than averages, and look to the local environment of the cluster for clues to the mechanisms.

We have observed that individual decaying particles shrink at various rates typically between $\tau^{1/6}$ and $\tau^{1/3}$, which are close to the classical Ostwald ripening theory prediction of $\tau^{1/4}$ or $\tau^{1/3}$ for decay of any one dimension. This observation is key to understanding the ripening process since when combined with the slow growth exponents for the ensemble it dictates that there must be a wide range of particle sizes in which growth or decay do not occur. This stable size regime is not present in the classical Ostwald or diffusion coalescence theories, and we can in any case rule out the latter as the particles are immobile.

4. Simulations for the spatial properties of the arrays and comparison with experiment

The identification of Ostwald-type processes dominating the overall ripening has implications for the spatial properties of the ripened nanoparticle arrays which we can investigate using simple coarse-grained models. In the simulations discussed below we do not attempt to include any of the atomistic complexities of adatom release and capture by nanoparticles; the experimental data shows how this impacts the dynamics of the ripening but we do not anticipate

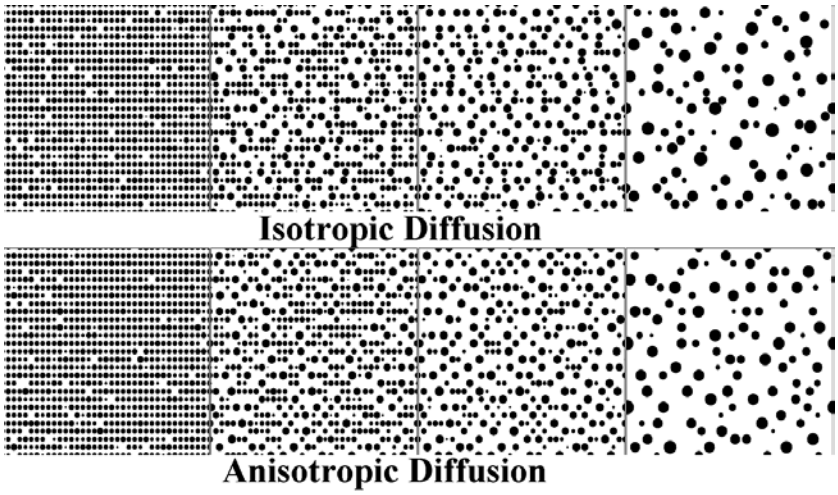

Figure 7. The simulated ripened array with nanoparticles shown by their footprint on the surface and taken as snapshots in the simulations at 900, 520, 300 and 100 particles. The anisotropic diffusion is 8 times faster in the vertical direction and leads to greater coalescence at early times and a slight preference for the staggering of nanoparticles in adjacent rows.

it strongly affecting spatial features. In previous work we have investigated the ripening of two-dimensional islands using coarse-grained, straightforward Monte Carlo simulations, finding that the system self-organizes into a statistically scale-invariant state irrespective of the size-dependence of the release rate [18], which agrees well with experimental data. The explanation for this behaviour is the dominance of 'local ripening', whereby the growth/decay of an island depends on its immediate environment because the diffusion length of adatoms is comparable to the inter-island separation. In a similar fashion we anticipate that the spatial properties of the ripened nanoparticle arrays reported here are dictated by local ripening, which any sensible coarse-grained model will reproduce.

In the simulation we chose to employ a lattice of (468×468) to represent the substrate, upon which monomers diffuse, with clusters initially positioned on a (13×18) array to mimic the microscopy image sizes and the starting experimental situation. The clusters are modelled as immobile hemispheres, with an initial radius of 5 monomers. They immediately change volume, and hence radius and footprint on the lattice, whenever a monomer attaches or detaches from them. Due to the stability of the nanoparticles, we assume that the ripening is limited by the monomer release rate as opposed to the diffusion-limited scenario of classical Ostwald ripening. In the algorithm, a monomer is released from a randomly chosen cluster and performs a random walk on the lattice until it encroaches upon any cluster's footprint, whereupon it is absorbed by that cluster. The process is repeated and over time some clusters shrink at the expense of their neighbours, as illustrated in figure 7. It is immediately clear that this simple simulation produces ripened arrays that compare well in a visual sense with those observed experimentally. Obviously the dynamics of the simulation do not have such a favourable comparison since the average cluster volume increases linearly with time (measured as the number of algorithmic iterations taken; CPU time for each iteration of course grows as the island density drops). Different power laws could be imposed by making the monomer release rate dependent on cluster size; however the experimental data displays a number of different regimes of behaviour that require a detailed atomistic investigation that has not yet been performed, and in any case our work on two-dimensional islands shows this does not affect spatial ordering.

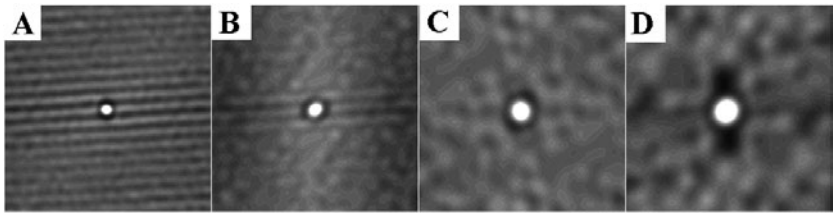

Figure 8. Height–height autocorrelation of the Pd nanoparticle covered surface imaged at four different ripening temperatures. The autocorrelation maps span ±500 Å about the origin, which is perfectly correlated (white). The numbers of particles quoted are per 1000 Å square image. (A) Pd nanocluster decorated surface with a density of 943 particles formed by nucleation and growth on the reconstructed surface at RT and imaged at 373 K. The near horizontal white stripes indicate the preference to form on the cross-links. (B) Imaged at 523 K with 670 particles, a clear denuded region is formed (dark ring) and the ordering on the cross-links sites is weakening. (C) By 773 K the particles and denuded region have grown, 285 particles. (D) after ripening at 873 K the surface arrangement shows a clear preference for large separation between particles in the ⟨001⟩ (vertical) direction, 128 particles.

One of the features that can easily be studied using the simulation is the impact of cluster coalescence whenever neighbours touch. In the upper panel of figure 7 the clusters remain spatially distinct and no coalescence is observed; this is because the initial cluster size, chosen by comparison with experiment in figure 1(A), is sufficiently small. However by inclusion of an anisotropic diffusion of the monomers on the lattice, coalescence is induced (see lower panel). The experimental substrate has a (1×2) reconstruction which might feasibly result in faster adatom diffusion in the ⟨001⟩ direction. When this anisotropy is included in the simulation, clusters can grow at the expense of their ⟨001⟩ nearest neighbours and then coalesce with their $\langle 1\bar{1}0\rangle$ neighbours. In figure 7 we show a sequence of arrays with a factor 8 difference in monomer diffusivity in the orthogonal directions (fast in the vertical ⟨001⟩). The proportion of coalescence events is now significant, with about 50% of the final ripened clusters having undergone coalescence at some point. Some spatial properties are slightly different when one visually compares isotropic and anisotropic cases, and we quantify some of the effects below.

Figure 8(A) shows the experimentally determined height–height autocorrelation functions for the cross-linked (1×2) surface decorated with Pd and ripened at a sequence of differing temperatures:

$$G(i, j) = \langle (z(x, y) - z(x + i, y + j))^2 \rangle. \tag{2}$$

The x and y co-ordinates correspond to points in the STM image of height $z(x, y)$ and the i, j co-ordinates to the correlation plots. The greyscale in the correlation plots shows white as total correlation ($G = 0$) and black as uncorrelated. Line profiles (not shown) in the two orthogonal directions of the autocorrelation plots indicate the periodicity of the nanoclusters likely to be found sitting on every other cross-link in the $\langle 1\bar{1}0\rangle$ direction and every cross-link in the longer ⟨001⟩ direction. A denuded region around each cluster is clear which indicates a minimum preferred cluster–cluster separation. The autocorrelation plots provide a useful diagnostic for the average local co-ordination of the supported nanoclusters. As the temperature is raised imposed spatial ordering is lost and at high temperature an anisotropic denuded region grows.

The height–height autocorrelation of the simulated arrays is shown in figure 9 for comparison with the experimental data of figure 8. Note that whilst the simulation is performed with periodic boundary conditions, the autocorrelation is produced without these for comparison with experimental data. Again the comparison is favourable when the monomer diffusion is isotropic with the formation of a denuded region. The lack of enhanced correlation between neighbours (as seen in the anisotropic model figure (C)) in the experiment suggests

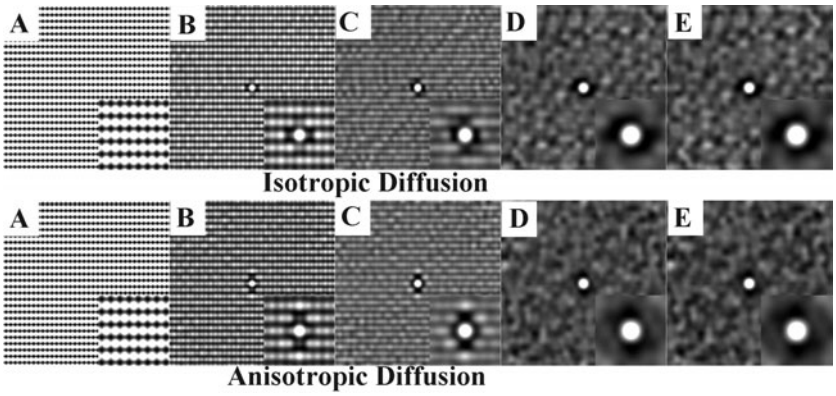

Figure 9. Height–height autocorrelation of the simulated arrays shown in figure 7, initially with 936 islands which is a comparable density to the initial state in the experiment. Correlation maps are taken at (A) 900 islands, (B) 520, (C) 300, (D) 100 and (E) 30.

that below 873 K the diffusion is not strongly anisotropic. In both theory and experiment the correlation length is a small multiple of the inter-island separation; as a consequence the local environment dominates, as discussed above, because adatoms rarely make excursions past the nearest neighbour of the parent island.

This conclusion is reinforced in the cluster size distributions. With significant coalescence the distribution has a bimodal character, whereas the experimental data has a single peak (at all temperatures [12]) as does the simulation for ripening with isotropic monomer diffusion shown in figure 10. We also compare the size distribution from the simulation to those derived from mean field theories (see appendix for details). In the classic mean field approach, (dotted curve) the island's growth rate is proportional to diameter only, yet this yields a distribution that is sharply peaked and narrow such that it does not extend much beyond scaled radius $\frac{s}{\langle s \rangle} \approx 1.5$. In the modified approach (solid curve) we take into account the correlation between island size and the number of nearest neighbours, and find a broader unimodal distribution.

In figure 10 we also show the experimental height distribution as well as the islands' radius distribution from the isotropic simulation taken at a comparable stage of the ripening. It should be noted that the mean field theories are for the asymptotic regime where the distribution is scale-invariant. It is difficult to truly reach this regime in experiment and simulation, since we require that the ripening island density reduces by many orders of magnitude which takes a long time and requires a lot of realizations for statistical purposes. However, it appears in figure 10 that the simulation data agrees well with the experimental data, and furthermore that the (Voronoi-inspired) modified mean field theory reproduces the radius distribution much better than the classic theory. In particular the form of the data is very similar to our modified theory, having a broad Gaussian shape with a tail that extends beyond $\frac{s}{\langle s \rangle} = 2$. This reinforces our intuition that whilst the detailed atomistic mechanisms of nanostructure ripening are absent from the simulations, the coarse-grained simulation is sufficient to reproduce salient features of the spatial properties of the ripened arrays.

5. Conclusion

We have followed the evolution of an array of TiO_2 supported Pd nanoparticles by *in situ* variable temperature STM. Ripening occurs with exponents indicative of a slow diffusion

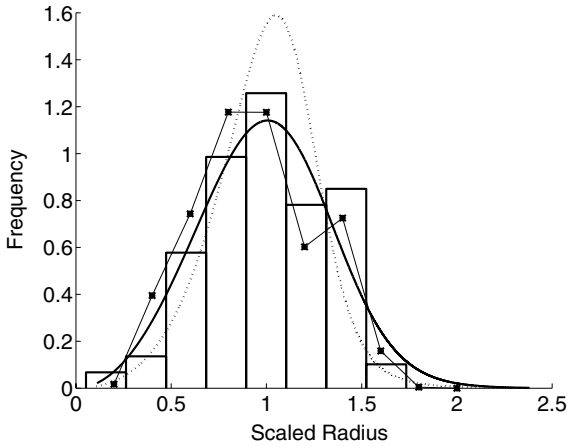

Figure 10. Scaled height normalized frequency distributions. The dotted curve shows the classic mean field theory ($P = 1/3$) result and the solid curve shows the new Voronoi-inspired theoretical shape ($P = 5/6$). The data points and thin lines are the results of a simulation run to near the final scaling state and the histogram shows the experimental result at 873 K where the array has also neared the scaling state. The simulations typically take 3 h CPU time on a 2 GHz machine, and 100 runs are used for the statistics.

coalescence regime, however, imaging shows particles are immobile and ripening is driven by inter-particle transport of material. Surprisingly the decay of some of the particles is rapid, reminiscent of Ostwald ripening, yet the whole array ripens slowly. The spatial distributions of the particles, assessed through autocorrelation functions, demonstrate that the initial ordering imposed by the lattice of nucleation sites decays and the nanoparticles develop exclusion zones around each other. The influence of anisotropy in diffusion is weak. Coarse-grained simulations of the system indicate that as the array ripens it self-organizes into a statistically scale-invariant state irrespective of atomistic detail. We introduce a theory to describe the particle size distributions characteristic of this state. Thus, providing a lattice of sites, which pin the nanoparticles, is insufficient to maintain an ordered array under conditions in which ripening takes place. This has obvious consequences for nanotechnological applications of arrays of supported structures that are in metastable states; surface diffusion will drive the system away from the ordered state towards a universal scale-invariant state of spatially correlated features.

Appendix. Modified mean field theory for the cluster size distribution

The classic mean field theory for cluster ripening limited by the monomer release rate models the monomer capture cross-section of a cluster as proportional to its radius. The growth rate of a cluster is then

$$v(s,t) = \frac{\mathrm{d}s}{\mathrm{d}t} = c\left(\frac{r}{\langle r\rangle} - 1\right),$$

where r is cluster radius, $\langle r\rangle$ is its average at any time t, s is the cluster size and c is monomer release rate. This law is used with the continuity equation for the time dependent distribution $f(s,t)$ of island sizes:

$$\frac{\partial f(s,t)}{\partial t} + \frac{\partial}{\partial s}[v(s,t)f(s,t)] = 0. \tag{A.1}$$

Analysis then yields an asymptotic scale-invariant island size distribution.

For the case of two-dimensional island ripening this theory does not produce a very satisfactory size distribution [18]. We found that the reason for this failure is that the mean field approximation inherent in the theory is not a good one. Instead the island sizes are strongly correlated with their Voronoi-type edge-cell area. This is a direct consequence of the 'local ripening' mechanism whereby substrate coverage is locally conserved. It follows that the number of nearest neighbours for an island is strongly correlated with its radius, so that larger islands receive monomers from more donors than smaller ones. This leads to a modified island growth law:

$$\frac{\mathrm{d}s}{\mathrm{d}t} = cw(z),$$

where $z = \frac{s}{\langle s \rangle}$ is the scaled size and, for two-dimensional islands,

$$w(z) = z - 1.$$

This results in the better island size distribution $\exp[-z]$ for detachment-limited ripening of two-dimensional islands.

We can easily modify the growth equations for the case of three-dimensional islands ripening on a two-dimensional substrate. The functional form of the growth law now reads:

$$w(z) = \left(\frac{z^{\mathrm{P}}}{M_{\mathrm{P}}} - 1\right), \tag{A.2}$$

where the power $P = \frac{1}{3}$ and $\frac{5}{6}$ respectively for the classic mean field and the Voronoi-derived scenarios. The latter arises because the Voronoi-type edge-cell area of each island is correlated to its size, and therefore its number of near-neighbour monomer donors varies as $s^{1/2}$. Combining with the island cross-section $s^{1/3}$ radius gives the $P = \frac{5}{6}$ growth law. In equation (A.2), M_{P} is the corresponding Pth moment of the resulting scaling distribution function.

The scaling solution to the continuity equation (equation (A.1)) can be expressed in terms of $w(z)$ (equation (A.2)) as follows:

$$F(z) = \frac{A}{Az - w(z)} \exp\left(\int_0^z \frac{-A\,\mathrm{d}z'}{Az' - w(z')}\right).$$

Here $F(z)$ is the usual distribution of scaled island sizes. The zeroth and first moments of $F(z)$ are one by construction, whereas the Pth moment must be found self-consistently since it enters into $w(z)$. For both cases of interest here ($P = \frac{1}{3}$ and $\frac{5}{6}$) a range of possible solutions have been found numerically, but the ones with the largest value A at size zero are assumed to be selected by the dynamics since these are the fastest-evolving solutions. These distributions are shown in figure 10 as a function of scaled radius for ease of comparison with the experimental height distributions.

References

[1] Zhdnov V P 2001 *Eur. Phys. J.* B **19** 97 and references therein
[2] Harris P J F 1995 *Int. Mater. Rev.* **40** 97
[3] Ostwald W 1900 *Z. Phys. Chem.* **34** 495
[4] Lo A and Skodje R T 2000 *J. Chem. Phys.* **112** 1966
[5] Jak M J J, Konstapel C, van Kreuningen A, Verhoeven J and Frenken J W M 2000 *Surf. Sci.* **457** 295
[6] Mitchell C E J, Howard A, Carney M and Egdell R G 2001 *Surf. Sci.* **490** 196
[7] Bennett R A, Stone P, Price N J and Bowker M 1999 *Phys. Rev. Lett.* **82** 3831
[8] Zhou J and Chen D A 2003 *Surf. Sci.* **527** 183

[9] Wahlström E, Lopez N, Schaub R, Thostrup P, Rønnau A, Africh C, Lægsgaard E, Norskøv J K and Besenbacher F 2003 *Phys. Rev. Lett.* **90** 026101
[10] Carrey J, Maurice J-L, Petroff F and Vaurès A 2001 *Phys. Rev. Lett.* **86** 4600
[11] Bowker M, Poulston S, Bennett R A, Stone P, Jones A H, Haq S and Hollins P 1998 *J. Mol. Catal.* A **131** 185
[12] Bennett R A, Newton M A, Smith R D, Evans J and Bowker M 2002 *Mater. Sci. Technol.* **18** 710
[13] Jak M J J, Konstapel C, van Kreuningen A, Verhoeven J, van Gastel R and Frenken J W M 2001 *Surf. Sci.* **494** 43
[14] Carrey J and Maurice J-L 2002 *Phys. Rev.* B **65** 205401
[15] Nichols F A and Mullins W W 1965 *J. Appl. Phys.* **36** 1826
[16] Nichols F A 1966 *J. Appl. Phys.* **37** 2805
[17] Combe N, Jensen P and Pimpinelli A 2000 *Phys. Rev. Lett.* **85** 110
[18] Tarr D M and Mulheran P A 2003 *Phys. Rev.* E at press